Submit to the journal *Catalysis Science & Technology*

Insights into Efficient Removal of Gaseous P-xylene Using Cerium-doped ZnO Nanoparticles through Photocatalytic Oxidation

Zhuowei Cheng[a], Junjie Wang[a], Dongzhi Chen[b], Jianming Yu*[a], Shihan Zhang[a], Shuang Wang[a], Yunfei Dai[a]

a College of Environment, Zhejiang University of Technology, Hangzhou, 310009, China

b Marine Science and Technology College, Zhejiang Ocean University, Zhoushan 316004, China

Corresponding author : Prof. Jianming Yu

Tel: 86-571-88320881; Fax: 86-571-88320882

E-mail: yjm@zjut.edu.cn

College of Environment, Zhejiang University of Technology, Hangzhou, 310009, China

Supporting Information

S1. Method for the synthesized catalysts and Gas chromatography

The chemical precipitation method was employed to synthesize ZnO and Ce-doped ZnO. For ZnO, 7.1895 g $ZnSO_4 \cdot 7H_2O$ was dissolved in 25 mL of ultrapure water, which was stirred vigorously using a stirrer. Then, 5.2995 g Na_2CO_3 in 50 mL ultrapure water was added drop by drop to the solution. Subsequently, the solution was stirred for 3 h (300 $r \cdot min^{-1}$), and the precipitate of ZnO was obtained. For Ce-doped ZnO, 4.34 g $Ce(NO_3)_3 \cdot 6H_2O$ was dissolved in 100 mL ultrapure water, and some were added to the $ZnSO_4 \cdot 7H_2O$ solution to prepare the mixed solutions (with Ce molar ratio of 0.5%, 1% and 1.5%). After adding the Na_2CO_3 solution drop by drop, the mixture was stirred for 3 h, and the precipitates of Ce-doped ZnO composite were obtained. All the prepared precursors were thoroughly washed three times with ethanol and ultrapure water, using ultrasonic bath (40 kHz) to make the precursors more dispersed, and were dried in air at 338 K overnight. The dried solids were calcined at different designated temperatures and duration to obtain the ZnO and Ce-doped ZnO. To coat the synthesized sample on the quartz boat, ethanol was used. After being mixed with ethanol, ZnO or Ce-doped ZnO was coated on the surface of quartz boat, and dried overnight in an oven at 338K.

Gas chromatography (GC, Agilent 7890, USA) with a flame ionization detector (FID) and a thermal conductivity detector (TCD) was used to measure the concentrations of p-xylene and CO_2, respectively. The FID was used to detect p-xylene; the temperatures of the injector, oven, and detector were set at 473 K, 373 K, and 453 K, respectively. The TCD was used to detect CO_2; the temperatures of the column and detector were set at 313 K and 473 K, respectively. Ozone concentration was determined by an ozone analyzer (XLA-BX-03, Shenzhen, China), and the

humidity of the hybrid gas was measured by a humidity meter (Testo 625, Germany) at the same time.

S2. Kinetic analysis using different PCO rate expressions

The Langmuir-Hinshelwood (L-H) model has been used because it can describe the PCO reaction happening on the gas-solid interface. Assuming that the surface reaction is the limiting step and that other byproducts have a weak effect on the active adsorption center of the catalyst, the L-H rate expression of p-xylene can be represented by the following rate equation [1,2].

$$r_{p-xylene} = I^n \cdot k\frac{K_{p-xylene}C_{p-xylene}}{1 + K_{p-xylene}C_{p-xylene}} \quad \text{(M1)}$$

Where I is the incident irradiance (2250 $W \cdot m^{-2}$), n is an incident irradiance exponential order constant (0.8), $c_{p\text{-}xylene}$ is the p-xylene initial concentration ($mg \cdot m^{-3}$), k represents the reaction kinetic constant ($(\mu g/(m^3 \cdot s))/(W \cdot m^{-2})^n$), and $K_{p\text{-}xylene}$ represents the equilibrium adsorption constant($m^3 \cdot mg^{-1}$) in a single site. This is usually called as L-H monomolecular model, which only considers the interactions between the reactant molecules and the catalyst surface.

In fact, the interactions between both the reactant and other reaction atmosphere components (water vapor, O_2) should be considered. Take water vapor for example. When dual adsorption happens on the same type of site, the model is based on competitive adsorption of reactant and water vapor molecules on equal type of sites. The rate expression can be determined:

$$r_{p-xylene} = I^n \cdot k\frac{K_{p-xylene}C_{p-xylene}K_wC_W}{\left(1 + K_{p-xylene}C_{p-xylene}K_wC_W\right)^2} \quad \text{(M2)}$$

Where K_w and C_w represent the H_2O adsorption equilibrium constant in a single site ($m^3 \cdot mg^{-1}$) and the H_2O gas phase concentration ($mg \cdot m^{-3}$), respectively. However, this model can be modified and rewritten as two different equations: if dual adsorption on two different types of sites of the

catalyst surface is considered without (M3) and with (M4) competition of reactant and water vapor molecules for the same type of site. In the present study, PCO rate of p-xylene can be described at steady-state as follows:

$$r_{p-xylene} = I^n k \frac{K_{p-xylene} C_{p-xylene} \quad K_w C_w}{1 + K_{p-xylene} C_{p-xylene} 1 + K_w C_w} \quad \text{(M3)}$$

$$r_{p-xylene} = I^n k \frac{K_{p-xylene,1} C_{p-xylene} \quad K_{w,2} C_w}{1 + K_{p-xylene,1} C_{p-xylene} + K_{w,1} C_w 1 + K_{p-xylene,2} C_{p-xylene} + K_{w,2} C_w} \quad \text{(M4)}$$

Where $K_{\text{p-xylene,1}}$, $K_{\text{p-xylene,2}}$, $K_{\text{w,1}}$ and K_{w},2 are the p-xylene and H_2O adsorption equilibrium constants ($m^3 \cdot mg^{-1}$) on the two types of sites (1 and 2), respectively.

S3. Ce-doped amount on the removal of p-xylene by Ce/ZnO under VUV

From Fig. S2, it could be found that Ce-doped amount had a great influence on the performance of such synthesized catalysts. When the doped amount increased from 0.1% to 1%, the removal efficiency of p-xylene was significantly enhanced, and the maximum efficiency of p-xylene reached >70%. However, when the doped amount continued to increase, the removal efficiency began to decrease. As a result, 1% Ce-doped amount was the best for p-xylene removal. The same applied to CO_2 generation and ozone decomposition. This might be due to Ce^{4+} or Ce^{3+} entered into the ZnO lattice to replace Zn^{2+} in the coprecipitation process, resulting in a large number of defects being formed in the ZnO lattice, with oxygen vacancies increasing. At the same time, such the increase also contributed to the separation of electron-hole pairs and prolonged the lifetime of ·OH [3]. In addition, Ce ions could also be used as electron storage to further enhance the photocatalytic effect. However, when the doped-amount was too much, Ce would capture a large number of electrons and holes, resulting in the lower photocatalytic performance. Based on these experimental data, the Ce-doped amount was chosen at 1%.

S4. Parameter calculation method in XRD and XPS analysis[4]

The crystallite size of the catalyst was calculated using the Debye-Scherrer equation (1):

$$D=0.9\lambda/\beta\cos\theta \quad (1)$$

Where λ is the wavelength of X-rays (λ=1.54 Å), θ is the diffraction angle and β is the full width at the half-maximum of the XRD line.

The volume of the sample hexagonal cell was calculated from the formula (2):

$$V=\frac{\sqrt{3}\,a^2c}{2}=0.866a^2c \quad (2)$$

For the wurtzite structure, the *u* is given by the formula (3):

$$u=\frac{a^2}{3c^2}+0.25 \quad (3)$$

The Zn-O bond length was calculated using the formula (4):

$$L=\sqrt{\frac{a^2}{3}+(\frac{1}{2}-u)^2c^2} \quad (4)$$

The relative ratios of Ce^{4+} and Ce^{3+} were calculated using the formulas (5) and (6):

$$[Ce^{3+}]=\frac{A_u'+A_v'}{A_u'''+A_u''+A_u'+A_u+A_v'''+A_v''+A_v'+A_v} \quad (5)$$

$$[Ce^{4+}]=\frac{A_u'''+A_u''+A_u+A_v'''+A_v''+A_v}{A_u'''+A_u''+A_u'+A_u+A_v'''+A_v''+A_v'+A_v} \quad (6)$$

S5. Some equations were involved in the process of photocatalysis.

Equations for the formation process of electron-hole (e^-/h^+) pairs generated on the catalyst:

$$ZnO + hv \rightarrow e^- + h^+ \quad (7)$$

$$e^- + O_2 \rightarrow \cdot O_2^- \quad (8)$$

$$h^+ + H_2O \rightarrow H^+ + \cdot OH \quad (9)$$

Equations for the inhibition of the recombination of e^-/h^+ pairs by the doped element Ce:

$$Ce^{4+} + e^- \rightarrow Ce^{3+} \quad (10)$$

$$Ce^{3+} + O_2 \rightarrow \cdot O_2^- + Ce^{4+} \quad (11)$$

Equations for the decomposition of ozone taking place on the catalyst:

$$O_3 + e^- \rightarrow O_3 \cdot^- \quad (12)$$

$$H^+ + O_3 \cdot^- \rightarrow HO_3 \cdot \quad (13)$$

$$HO_3 \cdot \rightarrow O_2 + \cdot OH \quad (14)$$

$$O_3 + V_0 \rightarrow O^{V_0} + O_2 \quad (15)$$

$$O^{V_0} + O_3 \rightarrow O_2^{V_0} + O_2 \quad (16)$$

$$O_2^{V_0} \rightarrow O_2 + V_0 \quad (17)$$

$$O_2^{V_0} + H_2O \rightarrow 2 \cdot OH + O^{V_0} \quad (18)$$

Where V_0 represents the catalytic active sites.

S6. RSM analysis for the removal of p-xylene by VUV-PCO

To analyze the influences of three factors (Ce doping ratio, calcination temperature and calcination duration) on the removal efficiency (RE) of p-xylene and the interactions among these synthesized parameters, the CCD and RSM method were used. Table S6 presents the real and coded values of the independent variables and their levels. A second-order polynomial model was used to fit the RE of p-xylene. Based on the analysis of variance (ANOVA), the obtained Fisher variation ratio and lack of fit were used for the evaluation of the relationships between process

variables and independent responses. Fig. S6 shows the fitted curve between the predicted and experimental values (with R^2=99.5%), further demonstrating the reliability of the model.

The Pareto analysis can determine the importance of each factor or the combined factors to the degradation efficiency of p-xylene. The influence of the single factor or the interaction factors on the response (degradation efficiency of p-xylene) can be determined based on the following equation:

$$P_i = \left(\frac{a_i^2}{\Sigma a_i^2}\right) \times 100 \quad (19)$$

Where Pi represents the percentage effect of single variable and a_i is statistical coefficients of Eq. (19).

Fig. S7 shows the Pareto analysis about the importance of synthesis parameters to p-xylene removal. Among these synthesized factors, the calcination temperature (b, 14.24%) was the most important parameter, followed by the calcination time (c, 0.88%) and Ce doping ratio (a, 0.11%). The thermo-gravimetric (TG) analysis of Ce-doped ZnO is shown in Fig. S8. The TG curve in the figure had three inflection points, which represented the loss of surface adsorbed water, the loss of crystallization water, and the loss of impurities (such as SO_4^{2-} and NO_3^-) adsorbed on the surface during the synthesis. According to the TG analysis, the calcination temperature had a strong influence on the crystal structure of catalyst, which tended to be stable within the range of 280 °C and 400 °C. Since a good crystal structure is much more important to the photocatalytic activity, the calcination process should be considered much more during the synthesis.

Fig. S9 (a-f) show the response 3D surface plot and 2D contour plot about the simultaneous influence of calcination temperature, calcination duration and Ce-doping ratio on p-xylene removal. An increase in the Ce-doping ratio (from 0.16% to 0.96%) enhanced the removal of p-

xylene; when the Ce-doping ratio further increased, the RE of p-xylene decreased. The reason was that excess Ce ions could also act as recombination centers for the e^-/h^+ pair, and such recombination could occur before the e^-/h^+ pair reacted with oxygen or water vapor [5]. As suggested before, a good crystal structure was a prerequisite for high photocatalytic activity and long stability of the catalyst. The best calcination temperature was 351 °C, indicating that a good lattice structure could be formed at this temperature. Calcination at lower temperature could not accelerate atomic diffusion, and not facilitate the crystal growth. As a result, a fully crystalline material did not be formed. A higher calcination temperature could accelerate the crystal growth rate, resulting in the collapse of pore structure, accompanying with the small specific surface area [6]. In addition, an optimum calcination time was necessary to avoid excessive catalyst sintering (compared to a prolonged calcination) and reduce carbon impurities (compared to shorter than optimum duration of calcination). Fig. S9a shows the 3D response surface (a) and contour plot (b) for the effects of calcination temperature and calcination time on the p-xylene removal. The contour plot was elliptical, indicating that the interaction between these two factors was significant [7]. The same was observed for the Ce doping ratio and the calcination temperature (Fig. S9b). Since the contour plot of the Ce doping ratio and calcination time was circular (Fig. S9d), the interaction between these two factors was negligible.

S7. Calculation method for p-xylene degradation percentage and ozone utilization extent.

The degradation percentage of p-xylene and the utilization extent of ozone in the present study were calculated by the following equation (20) and (21) :

$$Degradation\ precentage\ of\ p-xylene = \frac{C_{initial} - C_{out}}{C_{initial}} \times 100\% \quad (20)$$

$$Utilization\ extent\ of\ ozone = \frac{[O_3]_{VUV} - [O_3]_{out}}{[O_3]_{VUV}} \times 100\% \quad (21)$$

Where $C_{initial}$ represents the concentration of p-xylene in the inlet gas, C_{out} represents the concentration of p-xylene in the outlet gas; $[O_3]_{VUV}$ is the concentration of ozone in the outlet gas when there are no catalyst and no p-xylene; and $[O_3]_{out}$ is the concentration of ozone in the outlet gas when there were catalyst and p-xylene.

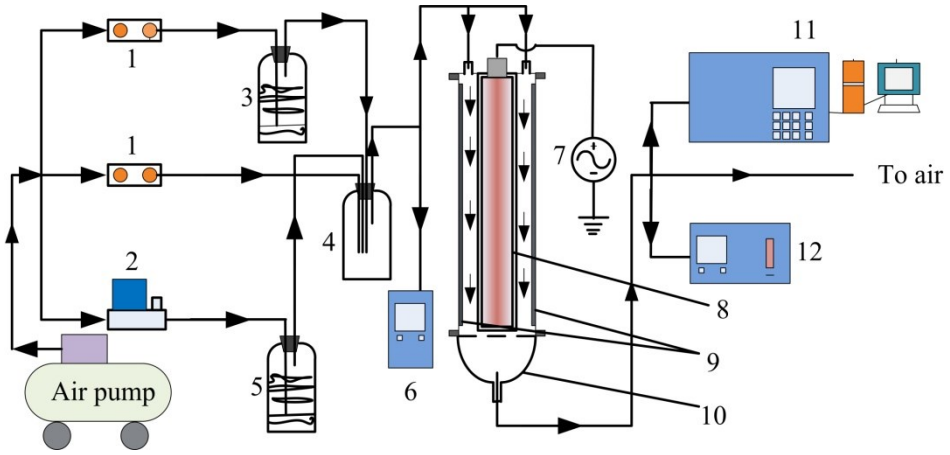

1. Rotor flowmweter; 2. Mass flow controller; 3. Water; 4. Mixer; 5. Paraxylene; 6. Humidity meter; 7. Power; 8. VUV lamps; 9. Catalyst layer; 10. Reactor; 11. GC; 12. Ozone analyzer

Fig. S1 The schematic diagram of the photo-reactor system.

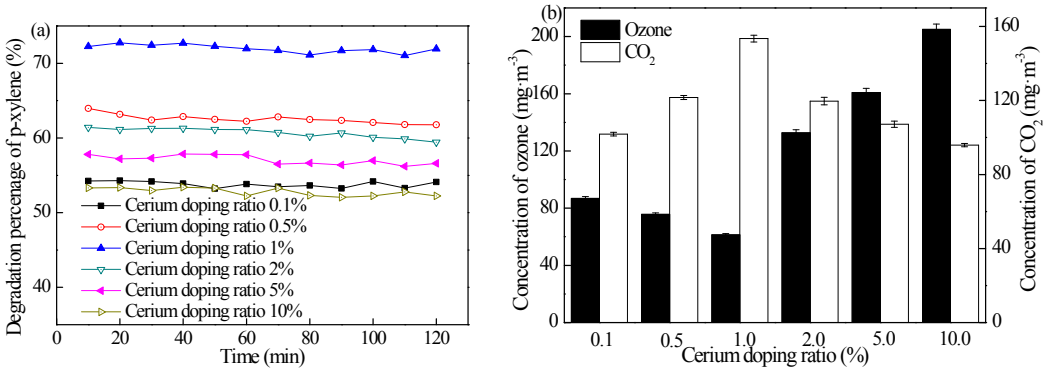

Fig. S2 Effect of different Ce-doped amounts on the removal efficiency of p-xylene (a), ozone and CO_2 concentration in the outlet (b).

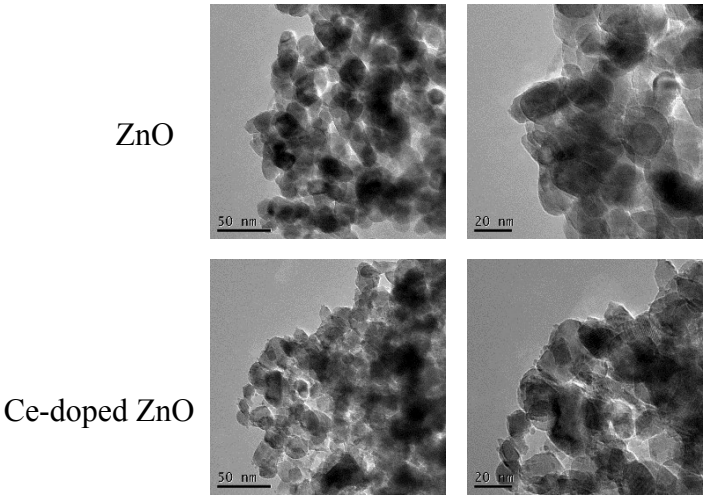

Fig. S3 TEM images of pure ZnO and Ce-doped ZnO.

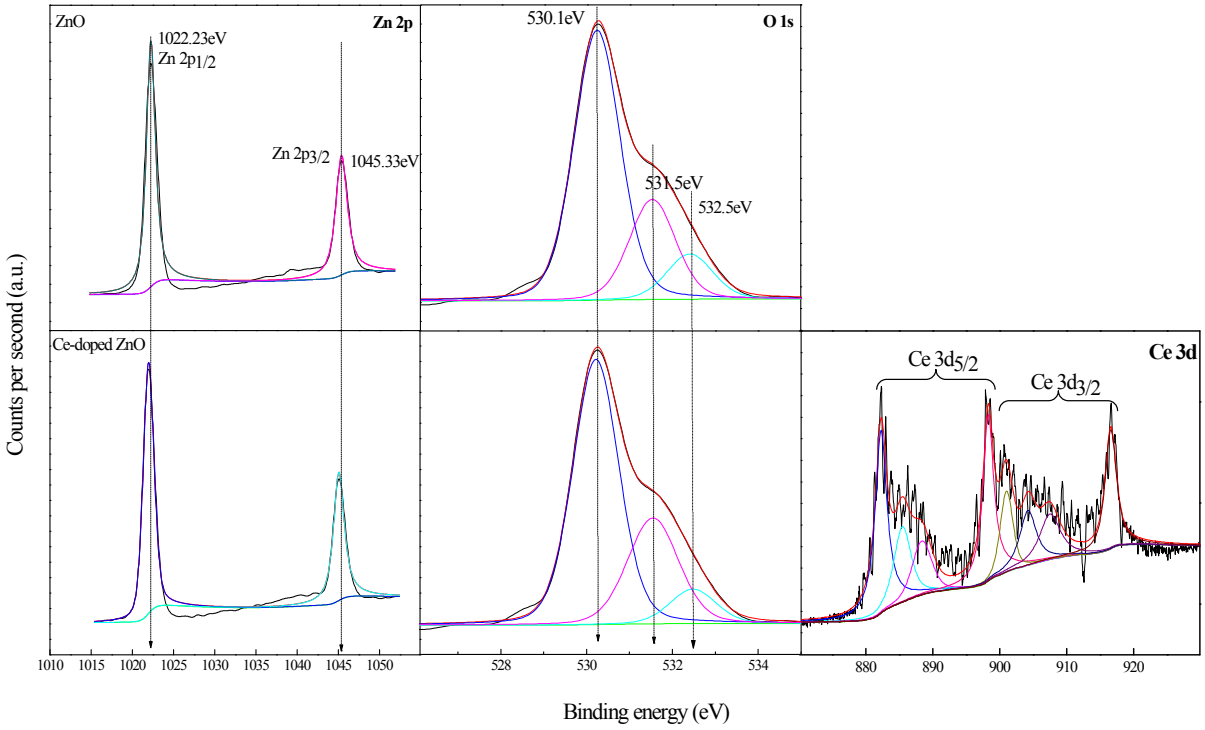

Fig. S4 XPS of Zn (2p), O (1s) and Ce (3d) nanoparticles.

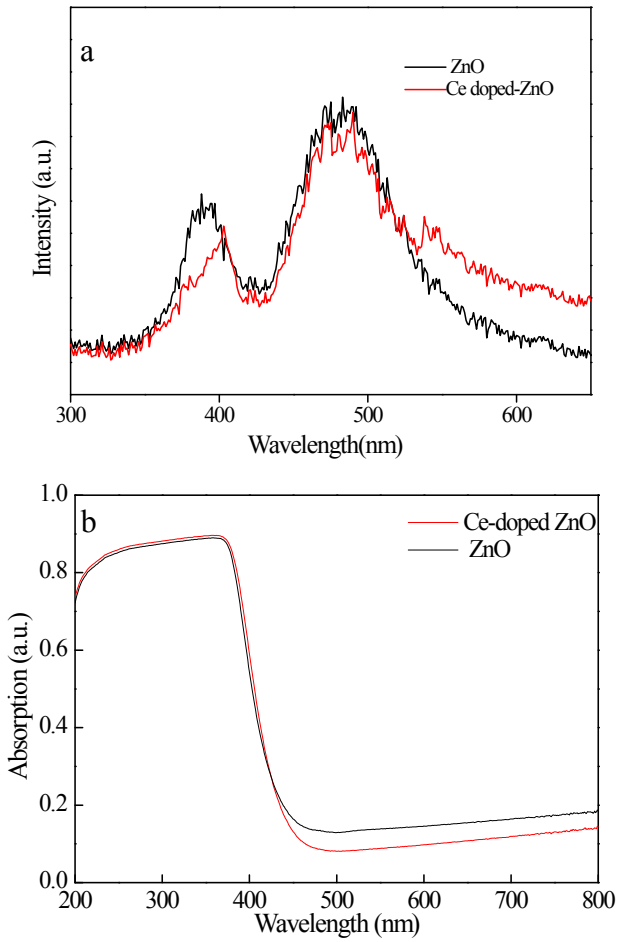

Fig.S5 Photoluminescence spectra (a) and UV-vis absorption spectra (b) of ZnO with or without Ce

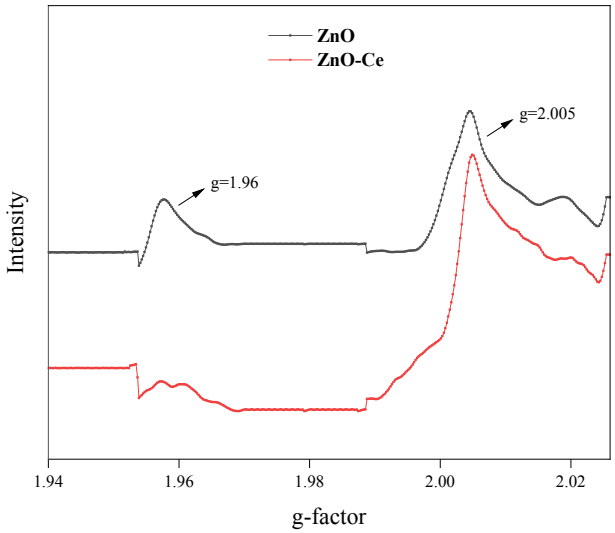

Fig. S6 EPR spectra of ZnO and 1% Ce-doped ZnO.

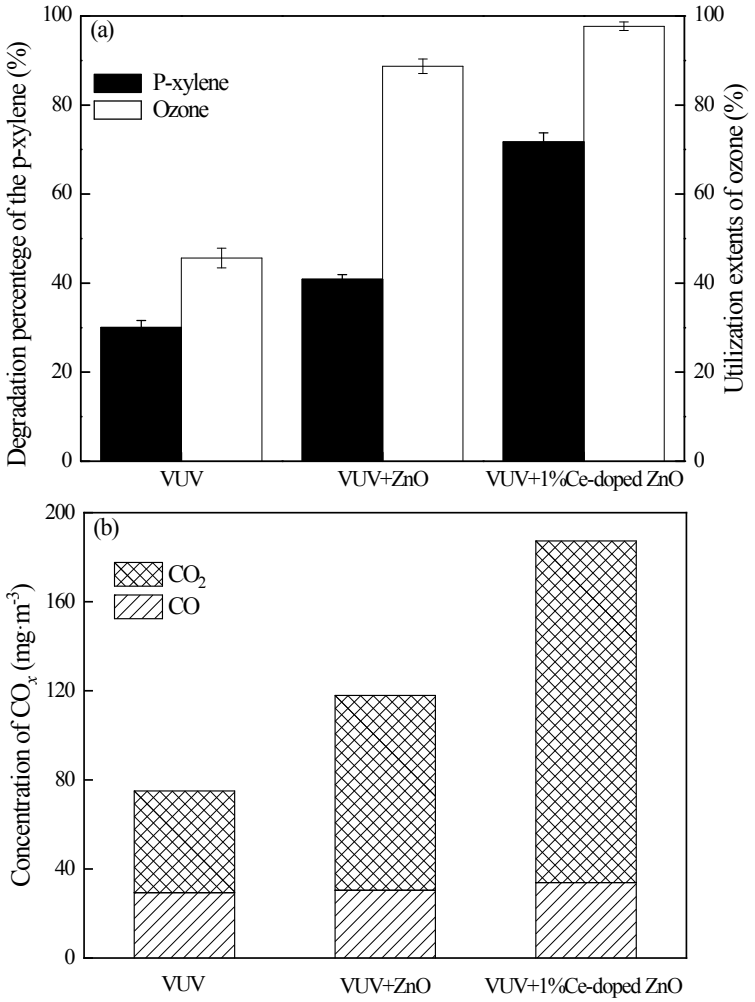

Fig. S7 The comparison of ozone utilization extents (a) and CO_x productions (b) for these reaction systems.

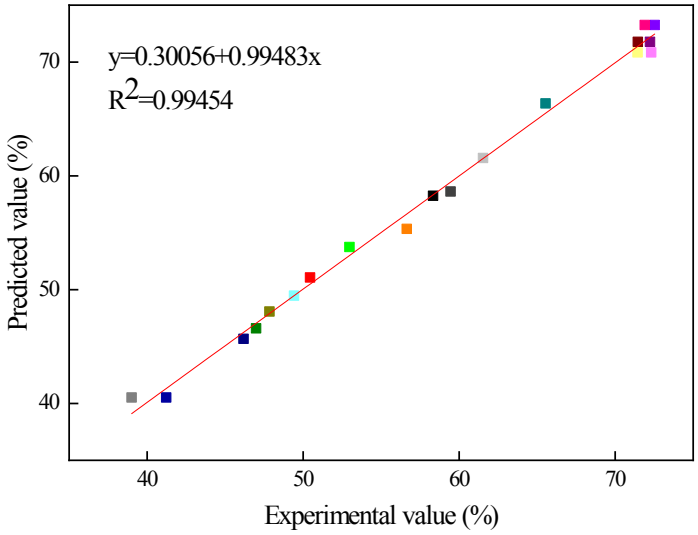

Fig. S8 Correlation between the experimental and predicted degradation efficiencies of p-xylene by Ce-doped ZnO under VUV irradiation.

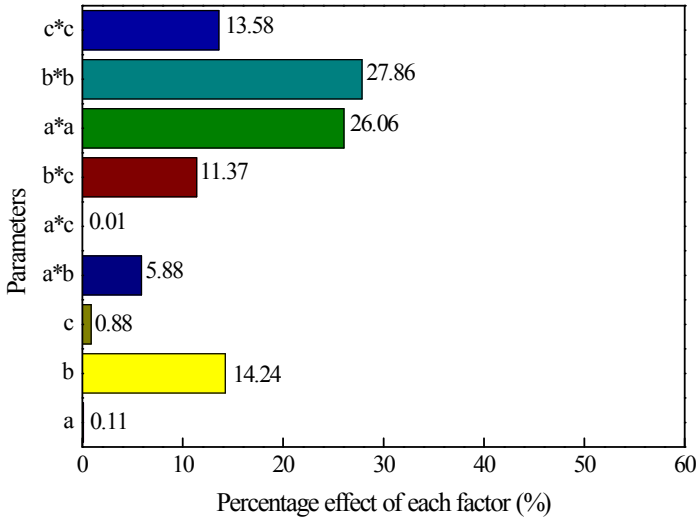

Fig. S9 Pareto graphic analysis for the importance assessment of each factor to the degradation efficiencies of p-xylene by Ce-doped ZnO under VUV irradiation.

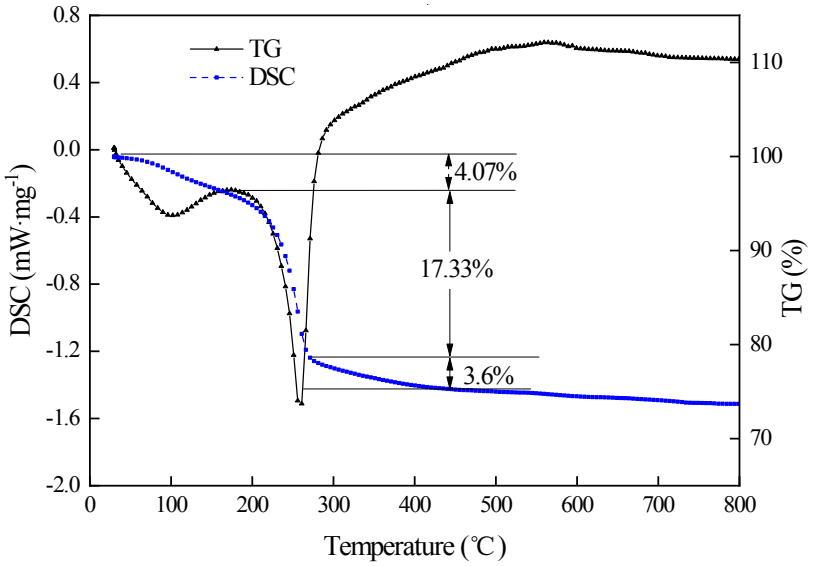

Fig. S10 Thermogravimetric analysis of the Ce-doped ZnO.

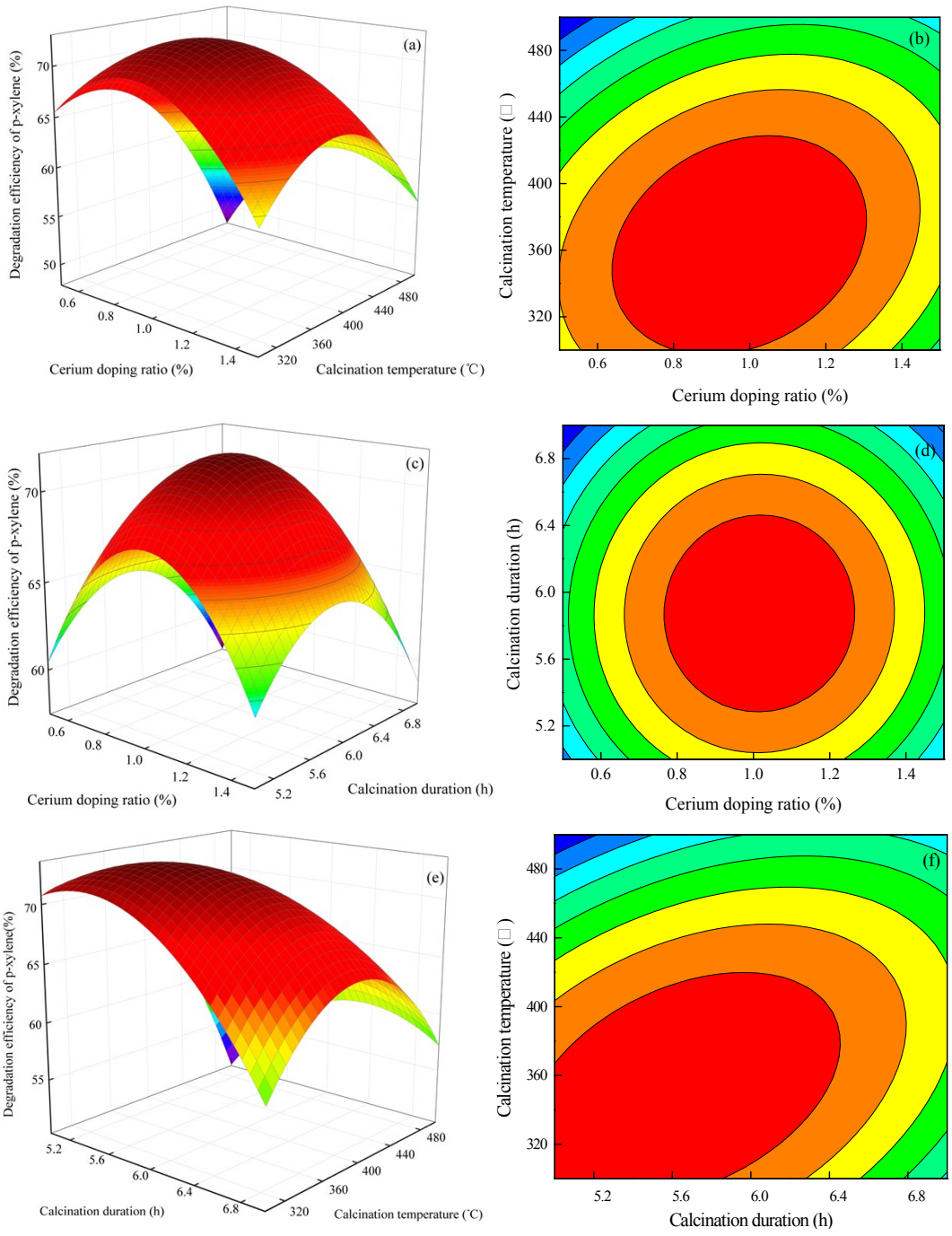

Fig. S11 Response 3D surface plot (a) and 2D contour plot (b) about the simultaneous influence of calcination temperature and calcination duration on p-xylene removal; response 3D surface plot (c) and 2D contour plot (d) about the simultaneous influence of calcination temperature and cerium doping ratio on p-xylene removal; response 3D surface plot (e) and 2D contour plot (f) about the simultaneous influence of calcination duration and cerium doping ratio on p-xylene removal.

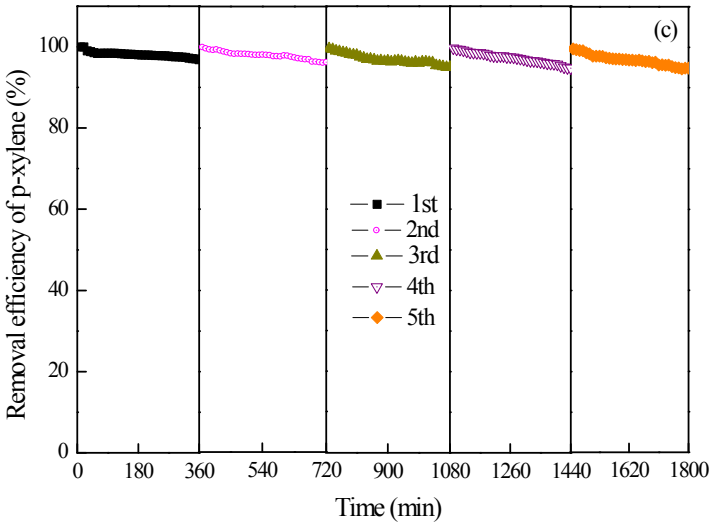

Fig. S12 Catalytic stability of the synthesized Ce-doped ZnO for p-xylene removal.

Table S1 X-ray diffraction parameter values of ZnO and Ce-doped ZnO.

Samples	2θ (º)	D (nm)	a=b (Å)	c (Å)	c/a	d (Å)	V (Å)^3	L (Å)
ZnO	36.231	21.369	3.249	5.205	1.602	2.475	47.58	1.977
1%Ce/ZnO	36.214	16.777	3.253	5.213	1.603	2.478	47.77	1.982

D refers to crystallite size of the sample.

a=b and c refers to Lattice parameter values of the sample.

c/a refers to Atomic packing factor of the sample.

d is the average crystallite dimension.

V refers to the unit cell volume.

L refers to Bond length (Zn-O).

Table S2 Comparison of FWHMs and peak area of de-convoluted peaks for the pure ZnO and Ce-doped ZnO

Element	Sample	Peaks eV	FWHM (Area)	Sample	Peaks eV	FWHM (Area)
Zn 2p	ZnO	1021.97	1.68	Ce-doped ZnO	1021.97	1.62
		1045.05	1.65		1045.05	1.58
O1s		530.1	1.47 (43486)		530.1	1.46 (41628)
		531.5	1.23 (20604)		531.5	1.25 (22058)
		532.5	1.18 (5409)		532.5	1.22 (5037)
Ce 3d		-	-		885.45-916.59	2.18-2.53

Table S3 Changes of O 1s before and after doped

	ZnO	Ce/ZnO
A(Lattice oxygen)	65.60	62.60
B(Absorbed water)	7.50	5.10
C(Oxygen vacancy)	26.90	32.40

Table S4 Actual and predicted values for the central composite design based on three experimental factors.

Run	Level of factors			Response (% degradation percentage)		Residual
	a	b	c	actual	predicted	
1	1.50	300	7	47.84	48.074	-0.22992
2	0.50	300	7	46.18	45.67	0.51435
3	1.00	400	6	72.23	71.77	0.46332
4	1.00	400	6	71.45	71.77	-0.31508
5	1.50	500	5	46.70	46.59	0.39339
6	0.50	300	5	65.54	66.37	-0.82606
7	0.50	500	5	41.23	40.52	0.71218
8	1.50	500	7	56.65	55.34	1.30832

9	1.00	400	6	72.53	73.26	-0.72460
10	1.00	400	6	71.90	73.26	-1.35270
11	0.50	300	7	55.32	55.23	0.08888
12	1.50	300	5	61.54	61.57	-0.03209
13	1.00	568	6	39.00	40.51	-1.51062
14	1.00	400	6	71.44	70.85	0.58992
15	0.16	400	6	49.41	49.47	-0.05890
16	1.00	400	6	72.31	70.85	1.46053
17	1.00	232	6	59.45	58.62	0.82714
18	1.00	400	4.32	58.33	58.25	0.08511
19	1.84	400	6	50.44	51.07	-0.62458
20	1.00	400	7.68	52.97	53.74	-0.76859

Table S5 Analysis of variance (ANOVA).

Source	Sum of squares	Degree of freedom	Mean square	F-value	P-value
Model	2368.13	9	263.13	168.54	<0.0001
Cerium doping ratio	3.07	1	3.07	1.96	0.1986
Calcinations temperature	396.40	1	396.40	253.90	<0.0001
Calcinations time	24.53	1	24.53	15.71	0.0042
Lack of Fit	11.61	5	2.32	7.92	0.0594
Residual	12.49	8	1.56	-	-
Total	2397.36	19	-	-	-

R^2=99.48%, Adj- R^2=98.89%

Table S6 Factor and their levels in central composite design.

Factors	symbol	Real values of coded levels				
		-α	-1	0	+1	+α
Cerium doping ratio (%)	a	0.16	0.50	1.00	1.50	1.84
Calcination temperature (℃)	b	232	300	400	500	568
Calcination time (h)	c	4.32	5.00	6.00	7.00	7.68

References

[1] F.V. Lopes, R.A. Monteiro, A.M. Silva, G.V. Silva, J.L. Faria, A.M. Mendes, V.J. Vilar, R.A. Boaventura, Insights into UV-TiO_2 photocatalytic degradation of PCE for air decontamination systems. Chem. Eng. J. 204 (2012) 244-257.

[2] F. V. Lopes, S. M. Miranda, R. A. Monteiro, S. D. Martins, A. M. Silva, J. L. Faria, R. A. Boaventura, V. J. Vilar, Perchloroethylene gas-phase degradation over titania-coated transparent monoliths. Appl. Catal. B-Environ. 140(2013) 444-456.

[3] S. P. Meshram, P. V. Adhyapak, S. K. Pardeshi, I. S. Mulla, D. P. Amalnerkar, Sonochemically generated Cerium doped ZnO nanorods for highly efficient photocatalytic dye degradation. Powder Technol. 318 (2017)120-127.

[4] R. A. Monteiro, F. V. Lopes, A. M. Silva, J. Ângelo, G. V. Silva, A. M. Mendes, R. A. Boaventura, V. J. Vilar, Are TiO_2-based exterior paints useful catalysts for gas-phase photooxidation processes? A case study on n-decane abatement for air detoxification. Appl. Catal. B-Environ. 147(2014) 988-999.

[5] S.P. Meshram, P.V. Adhyapak, S.K. Pardeshi, I.S. Mulla, D.P. Amalnerkar, Sonochemically generated cerium doped ZnO nanorods for highly efficient photocatalytic dye degradation. Powder Technol. 318(2017) 120-127.

[6] C. X. Tian, Y.Yang, H. Pu, Effect of calcination temperature on porous titania prepared from industrial titanyl sulfate solution. Appl. Surf. Sci. 257(2011) 8391-8395.

[7] M. Sleiman, D. Vildozo, C. Ferronato, J. M. Chovelon, Photocatalytic degradation of azo dye Metanil Yellow: optimization and kinetic modeling using a chemometric approach. Appl. Catal. B-Environ. 77(2007) 1-11.